



Research Article

Performance analysis of water-based drilling mud through rheological modeling

Lawrence I. Igbonekwu, Joseph T. Nwabanne, Matthew C. Menkiti, Chigozie F. Uzoh, Matthew N. Abonyi, Mary-jane C. Ezechukwu and Pascal E. Ohale.

Special Issue

A Themed Issue in Honour of Professor Onukwuli Okechukwu Dominic (FAS).

This special issue is dedicated to Professor Onukwuli Okechukwu Dominic (FAS), marking his retirement and celebrating a remarkable career. His legacy of exemplary scholarship, mentorship, and commitment to advancing knowledge is commemorated in this collection of works.

Edited by
Chinonso Hubert Achebe PhD.
Christian Emeka Okafor PhD.

Performance analysis of water-based drilling mud through rheological modeling

²Lawrence I. Igbonekwu, ¹Joseph T. Nwabanne, ¹Matthew C. Menkiti, ²Chigozie F. Uzoh,
¹Matthew N. Abonyi, ²Mary-jane C. Ezechukwu and ¹Pascal E. Ohale.

¹Department of Chemical Engineering, Nnamdi Azikiwe University, Awka Nigeria.

²Department of Petroleum Engineering, Nnamdi Azikiwe University, Awka Nigeria.

*Corresponding Author's E-mail: jt.nwabanne@unizik.edu.ng

Abstract

This study evaluates the rheological behavior of water-based drilling mud using four widely recognized rheological models: Power Law Rheological Model (PLRM), Bingham Plastic Rheological Model (BPRM), Herschel-Bulkley Rheological Model (HBRM), and Casson Rheological Model (CRM). Experimental data were collected, and shear stress predictions from each model were compared with measured values across varying shear rates. The CRM consistently demonstrated superior accuracy, achieving the lowest absolute average percentage error (AAPE) across samples: 5.54% for NC, 3.23% for NC1, 5.28% for NC2, and 5.23% for NC3, with corresponding standard deviations of 3.85, 2.34, 3.10, and 2.82, respectively. HBRM followed closely with AAPE values of 6.37% for NC, 3.26% for NC1, 5.66% for NC2, and 5.31% for NC3. Conversely, BPRM exhibited the poorest performance, with AAPE values as high as 43.21% for NC, 42.11% for NC1, 19.68% for NC2, and 42.45% for NC3, reflecting its limited predictive capability. These findings highlight the significance of accurate rheological modeling in managing viscosity and shear stress, critical factors in optimizing drilling fluid performance. The CRM's robust performance across a range of shear rates establishes it as the most reliable model for predicting the rheological properties of water-based drilling mud, offering valuable insights for improving drilling fluid design and operational efficiency.

Keywords: Drilling mud; Rheological models; shear rate; shear stress; BPRM, PLRM, CRM, HBRM

1. Introduction

Drilling mud, or drilling fluid, is an indispensable element in oil and gas drilling operations. Performing a wide range of critical functions assures safety and efficiency (Sarsenbaevna and Ospanovich, 2024). Among the major responsibilities are cooling and lubrication of the drill bit, transportation of cuttings from the wellbore, and wellbore stability (Pedrosa et al., 2021). The drilling mud also exerts hydrostatic pressure to prevent the intrusion of formation fluids and reduces the risk of blowouts (Chukwuemeka et al., 2017). These become especially crucial attributes in deep and difficult drilling environments where precision with control is critical to successful operations. The choice of drilling mud formulation will depend on the well's operational requirements and geological conditions (Aftab et al. 2017). Among all types of drilling fluids, water-based drilling mud, or WBM, has a wide application due to the fact that it is cheaper, simpler to formulate, and less of an environmental hazard than oil- or synthetic-based mud (Fakhari, 2022). Generally, WBMs are mixtures of fresh water as a base fluid with additives like clays, polymers, and chemicals to achieve desired performance properties, including viscosity and fluid loss/shale stabilization characteristics. These factors play an important role in maintaining drilling operations effectively and dependably.

Designing and formulating drilling mud, it is necessary to be familiar with the mud rheological properties—that are the relations which define fluid flow and its deformation under load (Chen, 2022). Rheology stands at the root of ensuring appropriate circulation of the drilling fluid and efficient cuttings removal from the wellbore (Klungtvedt, 2023). Properties such as viscosity, yield stress, and shear-thinning behavior directly have an impact on critical parameters like hole cleaning, pressure losses, and equivalent circulating density (Deng et al., 2020). Since most of the drilling fluids are non-Newtonian fluids, it is impossible to fully describe their flow characteristics with a simple Newtonian model (Irgens, 2014), which calls for a specialized rheological model. Rheological modeling has evolved over years with several different models being propounded to characterize flow properties of the drilling fluids. One of the most used models for describing shear-thinning behavior is the Power Law Rheological Model (Picchi, et al., 2017). The simplicity of the PLRM makes it attractive for practical applications, defining the relationship of shear stress to shear rate by a straightforward power-law equation. However, this is a serious drawback to the effectiveness of the PLRM in complicated drilling conditions since the model cannot predict fluid behavior at extreme shear rates (Sharma & Kudapa, 2021). Improved on this is the BPRM, which introduces the inclusion of yield stress as a parameter of the minimum stress a fluid must undergo to begin flowing (Mitsoulis and Tsamopoulos, 2017).

Despite this superior quality, the BPRM tends to overestimate shear stress at lower shear rates and thus becomes less representative while describing non-Newtonian fluids. In the light of overcoming these weaknesses, the Herschel-Bulkley Rheological Model (HBRM) was proposed. It couples the yield stress concept of BPRM with flexibility in a power-law relationship to better capture the behavior of shear-thinning fluids over a wider range of shear rates (Nollet & Toldrá, 2015). The HBRM will be more accurate, although it may deviate at extreme conditions. Another promising approach is the Casson Rheological Model (CRM), recognized to include both yield stress and plastic viscosity (Adewale et al., 2017). The CRM represents consistent and precise predictions at different shear rates and thus can be used for complex fluid systems. Precise rheological modeling of the drilling mud is critically important regarding operational efficiency. For example, poorly chosen models may have huge disadvantages for the process in terms of poor cuttings transport, excessive pressure losses, and formation damage. For example, underestimating viscosity at low shear rates results in poor removal of cuttings, while its overestimation at higher rates leads to energy wastage (Rostami, 2017). This is why it is so vital to choose the appropriate rheological model necessary for the purpose of guaranteeing the best operation with minimal hazards during drilling. This paper presents the rheological behavior of water-based drilling mud interpreted by four well-known models: PLRM, BPRM, HBRM, and CRM. Experimental data were collected for four formulations, namely NC, NC1, NC2, and NC3, which included specific additives to attain targeted properties.

The models have been evaluated based on the predicted shear stress values compared with experimental data for a wide range of shear rates. Accuracy and reproducibility of the models were established using metrics such as AAPE and standard deviation. Several studies have identified the weaknesses and strengths of various rheological models. For example, it has been pointed out by Adewale et al. (2017) that conventional models such as PLRM and BPRM fail to represent the complex behavior of non-Newtonian fluids. Based on these result, the research has made an extended comparison of the models to provide a better understanding of which model is best applied under specific operation conditions. The research importance deals with relevance to more sophistication and demand from modern drilling practices. That is, exploring deeper and more challenging reservoirs necessitates rheological modeling to achieve operational success. This therefore, contributes to developing optimized drilling fluids that will enhance wellbore operations with reduced drilling risk. This research covers the critical gaps in drilling fluid engineering by providing a framework for the selection of the most appropriate rheological model for water-based drilling mud. Experimental validation and robust analysis are presented in this work to translate into actionable insights on how to improve fluid design and application. The findings will have important implications for the petroleum industry, paving the way for more efficient, sustainable, and reliable drilling.

2.0 Materials and methods

Randomly collected local clay (NC) samples from Nteje in Oyi local government of Anambra, Nigeria was oven-dried and milled to remove excess moisture then reduce to fine particle size and labelled as NC. A portion of NC was beneficiated via wet and dry method of beneficiation as described by James et al., (2008). The result of the beneficiation gave rise to NC1, NC2 and NC3. Drilling fluid was prepared in accordance to API standard of 22.5g of clay sample in 350ml of distil water and was further beneficiated with 0.6g of poly anionic cellulose (PACR). Both the measured distil water and the weighed bentonite was transferred into the steel cup of the fann multi – mixer equipment and was vigorously agitated for about 20 minutes, until homogenous mixture is obtained. The mixture

was then allowed to stand for 24 hours for proper hydration and aging (Chu, and Lin, 2019). There after various viscosity dial reading ranging from 3rpm to 600rpm were determined using model 35 fann rotary viscometer. The process of washing, drying, heating, grinding and sieving of the local clay sample were carried out at Chemical Engineering laboratory Nnamdi Azikiwe University Awka,, Anambra state, Nigeria.

2.1 Rheological Model of Drilling Fluids

In drilling fluid, there is some internal resistance to overcome in order to move fluid from a static condition. The ratio of the shear stress (τ) to the shear rate (γ) is known as the fluid's viscosity (μ).

Mathematically,
$$\mu = \frac{\tau}{\gamma} \tag{1}$$

Viscosity is measured in units such as Newton-seconds per square meter (Ns/m²), Pascal-seconds (Pa-s), or poise (dyne-seconds per square centimeter, dyne·s/cm²). In a similar context, shear stress (τ) refers to the force necessary to maintain the flow of a specific fluid across a given area.

Shear stress (τ) =
$$\frac{F}{A} \tag{2}$$

Where;

F is the force applied measured in Newton, and A is the surface area measured in m²

The unit of shear stress is N/m²

Shear rate describes how quickly the velocity changes as one layer of fluid moves past a neighboring layer, divided by the distance separating the two layers (Krishna et al., 2019).

Mathematically,
$$= \frac{velocity}{distance} \tag{2b}$$

It is expressed in sec⁻¹ (reciprocal seconds).

RPM can be converted to sec⁻¹ by using the equation:

(rpm) = 1.703 γ (sec⁻¹) (Adewale, et al., 2017)

2.1.1 Power Law Model

The power law model is commonly used to characterize non-Newtonian fluids, where the relationship between shear stress and shear rate forms a curve known as the "consistency curve." This behavior is mathematically represented by an exponential equation, as shown in Equation 3.

$$\tau = k\gamma^n \tag{3}$$

The linear form of equation 3 is stated below

$$\log\tau = \log k + n\log\gamma \tag{3b}$$

Where;

K is the consistency coefficient (viscosity index) with unit of lb/100ft².Sⁿ. By multiplying k by a factor of 0.51 the unit can be converted to Pa.Sⁿ. Also n which is the fluid flow behaviour index shows the tendency of a fluid to shear thin and it is dimensionless. if n > 1, then the fluid is shear thickening and if n < 1, the fluid is shear thinning (Adewale et al., 2017).

K and n being the parameter can be evaluated graphically by a plot of log τ against log γ with log k as the resulting straight line's intercept and n as the slope. Alternatively k and n can also be evaluated from the following equations.

$$n = 3.32 \log (\text{reading at } 600 \div \text{reading at } 300) \tag{4}$$

$$K = 5.11 (\text{reading at } 300 \div 511^n) \tag{5}$$

A linear regression or curve fitting of log τ versus log γ can be used to determine the statistically optimal values of k and n. However, a significant limitation of the Power Law fluid model is that it assumes shear stress to be zero at a

zero shear rate, which is not an accurate representation of drilling mud. Drilling mud exhibits a residual shear strength even at a zero shear rate (Becker et al., 2003).

2.1.2 Bingham Plastic Model

The Bingham plastic model is one of the most widely used fluid models for analyzing the rheology of non-Newtonian fluids. This model assumes a linear relationship between shear stress and shear rate. The point at which the shear rate becomes zero is referred to as the "yield point" or threshold stress. Additionally, the slope of the curve representing shear stress versus shear rate is known as "plastic viscosity." While the Bingham plastic model provides satisfactory results for diagnosing drilling mud, it lacks the precision required for hydraulic calculations.

Plastic Viscosity (PV) can be determined by the following formula;

$$\text{Plastic Viscosity (PV)} = PV = \theta_{600} - \theta_{300} \quad 6$$

The unit is centipoise (cp)

Yield Point (YP) can be determined by the following formula, (equation 7);

$$\text{Yield Point (YP)} = \theta_{300} - PV \quad 7$$

The unit is lb. /100ft² or Pa.s

The Bingham plastic model, a two-parameter model, is extensively utilized in the drilling fluid industry to characterize the flow behavior of various types of muds. Its mathematical representation is given as:

$$\tau = \tau_0 + \mu_p \gamma \quad 8$$

Where μ_p is the plastic viscosity and the unit is mPa.s (cp) and τ_0 is the yield point with a unit of lb. /100ft² or Pa.sⁿ.

The two parameters μ_p and τ_0 can be determined from equations 6 and 7 respectively.

Fluids demonstrating Bingham Plastic behavior are defined by a yield point (τ_0) and plastic viscosity (μ_p) both of which remain unaffected by changes in shear rate. However, this model does not accurately capture the behavior of drilling fluids under extremely high shear rates near the drill bit or very low shear rates within the annulus. The parameters τ_0 and μ_p can be obtained from a plot of τ against γ where the intercept of the straight line corresponds to τ_0 and the slope represents μ_p . Alternatively, these parameters can also be calculated using equations 6 and 7, respectively.

2.1.3 Herschel Buckley

The Herschel-Bulkley model is an enhancement of the Power Law fluid model, designed to better capture the actual behavior of drilling fluids at low shear rates by incorporating an initial shear stress value. This model can be expressed mathematically as follows:

$$\tau = \tau_{0H} + k_H \gamma^{n_H} \quad 9$$

The linear form of equation 9 is given below;

$$\text{Log} (\tau - \tau_{0H}) = \log k + n \log \gamma \quad 10$$

Where k_H is the HRBM consistency index in (Pa.sn) and γ is the shear rate (s⁻¹), τ is the shear stress (Pa), τ_{0H} is the HRBM yield stress (Pa) and n_H is the flow behaviour index (dimensionless)

The yield stress is normally taken from value of 3rpm viscometer reading and the n_H and k_H values are calculated from the 600 or 300 rpm values or a plot of $\log (\tau - \tau_{0H})$ versus $\log (\gamma)$ will result in a straight line with intercept $\log k_H$ and slope n_H respectively. The Bingham Plastic model cannot effectively represent fluids exhibiting a yield point and strain-or stress-dependent viscosity. This limitation can be addressed in the Herschel-Bulkley model by replacing the plastic viscosity term in the Bingham Plastic model with a power-law expression. However, the concept of yield stress has been debated, as fluids may exhibit slight deformation even at stress levels below the yield stress.

2.1.4 The Casson Rheological Model

Visco-elastic fluid flow is described using the structure-based Casson rheological model (Anawe, & Folayan, 2018). This model has a more gradual transition from Newtonian to the yield region. Mathematically, the Casson model is expressed as;

$$\tau^{1/2} = k_{oc}^{1/2} + k_c^{1/2}\gamma^{1/2} \tag{11}$$

From equation 11, k_c represents the Casson plastic viscosity in mPa.s, and k_{oc} denotes the Casson yield stress in Pa.s. The parameters k_{oc} and k_c can be determined from the straight line obtained by plotting the square root of shear stress ($\tau^{0.5}$) against the square root of shear rate ($\gamma^{0.5}$). The slope of the line is $k_c^{1/2}$, and the intercept is $k_{oc}^{1/2}$. The Casson yield stress is calculated as the square of the intercept, $\tau_{oc} = (k_{oc})^2$ and the Casson plastic viscosity is the square of the slope $\eta_{ca} = (k_c)^2$

2.1.5 The measurement of model divergence from the model stresses

The degree to which each model deviated from the measured stresses was predicted using the following statistical techniques;

1. Absolute Average Percentage Error ϵ_{AAP} , given by the following equation;

$$\epsilon_{AAP} = [1/N \sum |(\tau_{measured} - \tau_{calculated}) / \tau_{measured}|] * 100 \tag{12}$$

2. The standard deviation of average percentage error which is obtained using the following Equation;

$$SD\epsilon_{AAP} = \sqrt{\sum (\epsilon\%error - \epsilon_{AAP})^2 / \sum f} \tag{13}$$

3.0 Result and Discussion

3.1 Analysis of NC + 0.6g PACR Mud Sample.

Table 1: Viscometer Readings for NC + 0.6g PACR. Power law

Speed (RPM)	Dial readings (lb/100ft ²)	Shear stress (τ) (pa)	Shear rate (γ) (s ⁻¹)	log τ	log γ	log ($\tau - \tau_{oH}$)	$\tau^{0.5}$	$\gamma^{0.5}$
600	29	14.79	1022	1.17	3.01	1.07	3.85	31.97
300	21	10.71	511	1.03	2.71	0.88	3.27	22.61
200	19	9.69	340.60	0.99	2.53	0.82	3.11	18.46
100	15	7.65	170.30	0.88	2.23	0.66	2.77	13.05
60	11	5.61	102.18	0.75	2.01	0.41	2.37	10.11
30	9	4.59	51.09	0.66	1.71	0.18	2.14	7.15
6	7	3.57	10.22	0.55	1.01	-0.29	1.89	3.20
3	6	3.06	5.11	0.49	0.708	0	1.75	2.26

3.1.1 Determining Model Parameters for NC1 + 0.6g PACR

The parameters of the power law rheological model (n and k), were determined through regression analysis using Equation (8). By plotting log τ against log γ , as illustrated in Fig.1, a straight line is obtained, represented by Equation (14):

$$\text{Log}\tau = 0.2931\text{log}\gamma + 0.2318 \tag{14}$$

Therefore, the power law equation for NC + 0.6g PACR can be expressed as:

$$\tau = 1.71\gamma^{0.2931} \quad 15$$

Equation (15) was used to calculate the power law stress values, which are recorded in Table 2. For the Bingham plastic model, the yield stress (τ_o) was determined using Equation (7), which gave a value of 13 lb/100ft². This value was converted to Pascals by multiplying by 0.51. The plastic viscosity was determined using Equation (6), resulting in a value of 0.0041 mPa·s. As a result, the Bingham plastic stress model for NC + 0.6g PACR is expressed as:

$$\tau = 6.63 + 0.0041\gamma \quad 16$$

Equation (16) was used to calculate the Bingham plastic stresses, which are presented in Table 2. The Herschel-Bulkley yield stress (τ_{oH}) was taken as the 3rpm viscosity reading from a viscometer, which is 3.06 Pa. The flow behavior index and consistency index were determined through regression analysis using Equation (10). A plot of $\log(\tau - \tau_{oH})$ versus $\log \gamma$ as shown in Fig. 2, yielded a straight line described by Equation (17):

$$\text{Log}(\tau - \tau_{oH}) = 0.6952 \log \gamma - 0.9777. \quad 17$$

Thus, the Herschel-Bulkley equation for NC + 0.6g PACR is written as:

$$\tau = 3.06 + 0.11(\gamma^{0.6952}) \quad 18$$

Equation (18) was used to calculate the Herschel-Bulkley stresses, as shown in Table 2.

The Casson yield stress (k_{oc}) and the Casson plastic viscosity (k_c) were determined from the plot of $\tau^{0.5}$ versus $\gamma^{0.5}$, as shown in Fig. 3. From this plot, the Casson's model equation for NC + 0.6g PACR is expressed as:

$$\tau^{0.5} = 2.81^{0.5} + 0.0051^{0.5}(\gamma^{0.5}) \quad 19$$

Equation (19) was used to compute the Casson stresses, which are shown in Table 2.

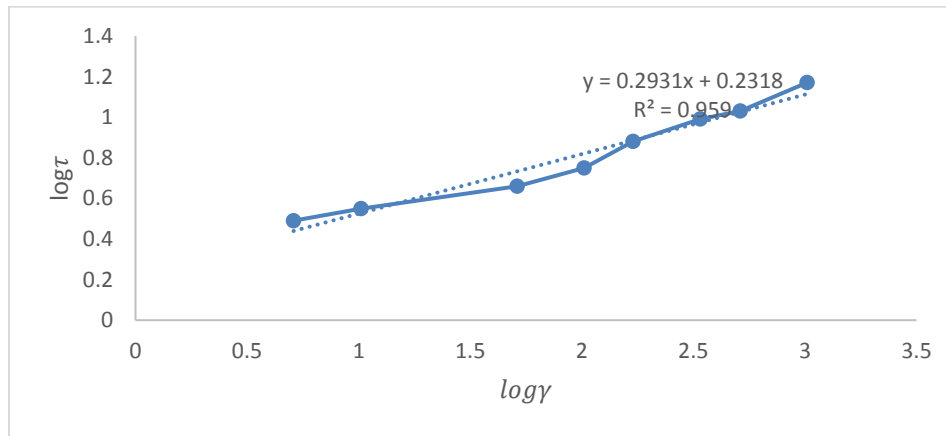


Figure 1: Power law Rheogram for NC + 0.6g PACR.

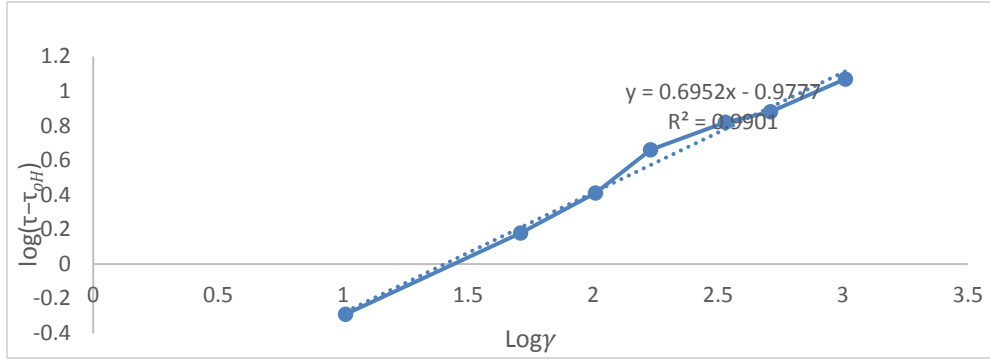


Figure 2: Hershel-Buckley Rheogram for NC + 0.6g PACR.

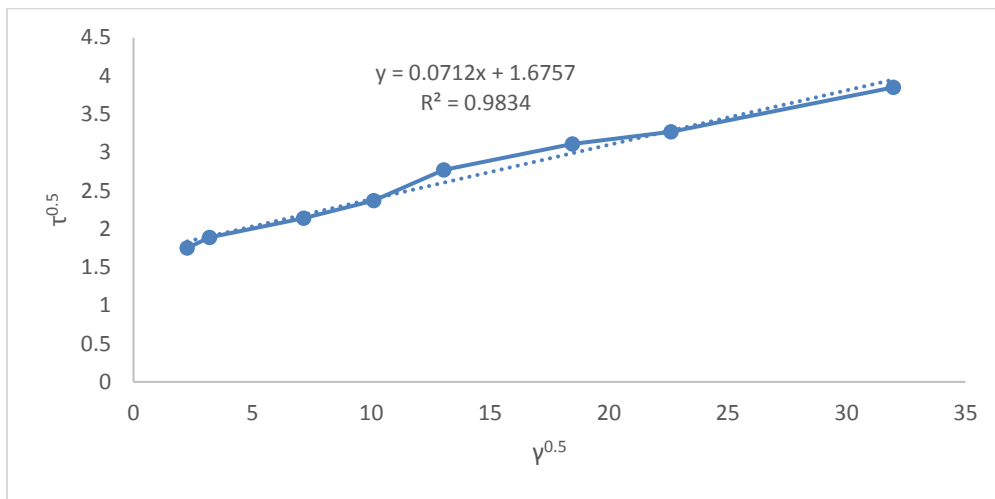


Figure 3: Casson Rheogram for NC + 0.6g PACR.

Table 2: Stress Values of Different Models for NC + 0.6g PACR Mud.

Speed (RPM)	Dial readings (lb/100ft ²)	Shear rate (s ⁻¹)	Measured (Pa)	PLRM (Pa)	BPRM (Pa)	HBRM (Pa)	CRM (Pa)
600	29	1022	14.79	13.03365	10.8202	16.66075	15.67629
300	21	511	10.71	10.63737	8.7251	11.46015	10.82836
200	19	340.60	9.69	9.444892	8.02646	9.395912	8.96572
100	15	170.30	7.65	7.708416	7.32823	6.97321	6.802994
60	11	102.18	5.61	6.636533	7.048938	5.803493	5.751318
30	9	51.09	4.59	5.416383	6.839469	4.754446	4.781899
6	7	10.22	3.57	3.379607	6.671902	3.613558	3.627531
3	6	5.11	3.06	2.758254	6.650951	3.40189	3.377287

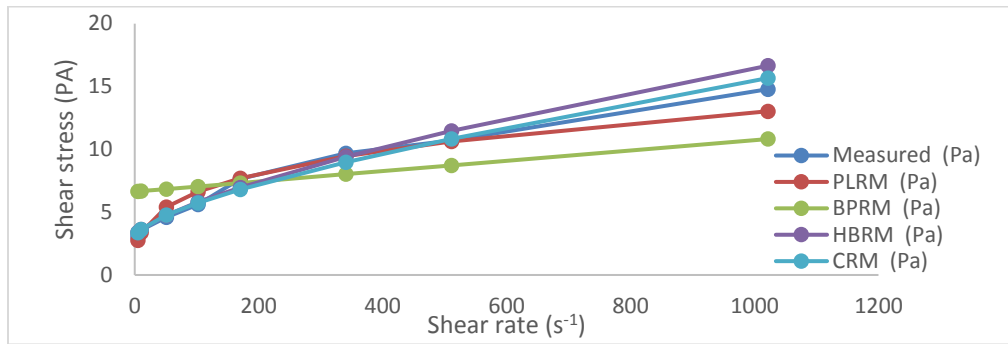


Figure 4: Shear Stress-Shear Rate Graph of Different Models for NC + 0.6g PACR

3.2 Analysis of NC1 + 0.6g PACR Mud Sample.

Table 3: Viscometer Readings for NC1 + 0.6g PACR.

Speed (RPM)	Dial readings (lb/100ft ²)	Shear stress (τ) (pa)	Shear rate (γ) (s ⁻¹)	$\log \tau$	$\log \gamma$	$\log (\tau - \tau_{oH})$	$\tau^{0.5}$	$\gamma^{0.5}$
600	57	29.07	1022	1.46	3.01	1.30	5.39	31.97
300	47	23.97	511	1.38	2.71	1.17	4.90	22.61
200	39	19.89	340.60	1.30	2.53	1.03	4.46	18.46
100	33	16.83	170.30	1.23	2.23	0.88	4.10	13.05
60	27	13.77	102.18	1.14	2.01	0.66	3.71	10.11
30	24	12.24	51.09	1.09	1.71	0.49	3.50	7.15
6	20	10.2	10.22	1.01	1.01	0.01	3.19	3.20
3	18	9.18	5.11	0.96	0.708		3.03	2.26

3.2.1 Determining Model Parameters for NC1 + 0.6g PACR

The parameters n and k for the power law model were derived by plotting $\log \tau$ against $\log \gamma$, as shown in Figure 5. This resulted in a straight line with the following equation (Equation 20):

$$\text{Log} \tau = 0.2134 \log \gamma + 0.7717 \quad 20$$

Thus, the Power Law Rheological Model (PLRM) for NC1 + 0.6g PACR can be expressed as:

$$\tau = 5.911 \gamma^{0.2134} \quad 21$$

Equation (21) was used to calculate the power law stresses presented in Table 4.

The plastic viscosity was determined using Equation (6), yielding a value of 0.0051 mPa·s, while the yield stress, calculated from Equation (7), is 18.87 Pa. Consequently, the Bingham Plastic equation for NC1 + 0.6g PACR is:

$$\tau = 18.87 + 0.0051 \gamma \quad 22$$

Equation (22) was used to derive the Bingham Plastic stresses listed in Table 4.

For the Herschel-Bulkley model, the straight-line equation obtained from plotting $\log(\tau - \tau_{0H})$ against $\log \gamma$, as shown in Figure 6, is:

$$\text{Log}(\tau - \tau_{0H}) = 0.6594 \log \gamma - 0.6413 \tag{23}$$

Thus, the Herschel-Bulkley equation for NC1 + 0.6g PACR is:

$$\tau = 9.18 + 0.23 (\gamma^{0.6594}) \tag{24}$$

Equation (24) was used to compute the stress values for the Herschel-Bulkley model in Table 4. Additionally, the equation for the straight-line plot of $\tau^{0.5}$ versus $\gamma^{0.5}$ for the Casson model, as shown in Figure 7, is:

$$\tau^{0.5} = 8.6^{0.5} + 0.0066^{0.5} (\gamma^{0.5}) \tag{25}$$

Equation (25) was used to generate the Casson model stresses presented in Table 4

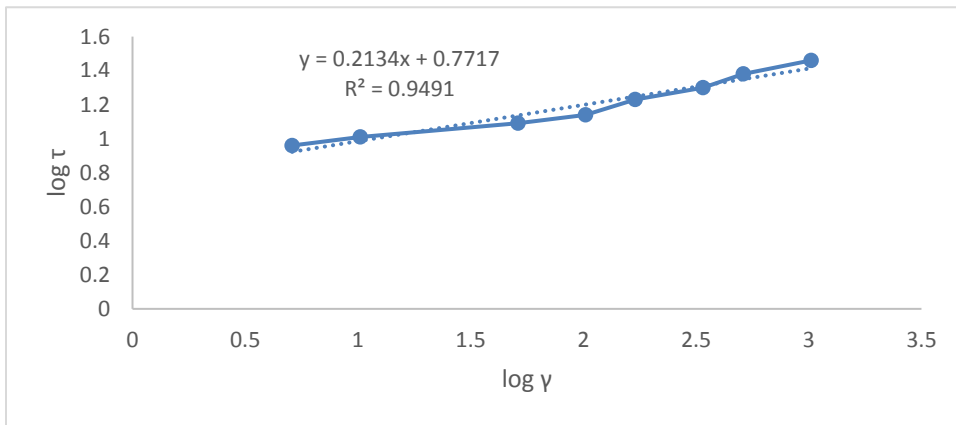


Figure 5: Power Law Rheogram for NC1 + 0.6g PACR

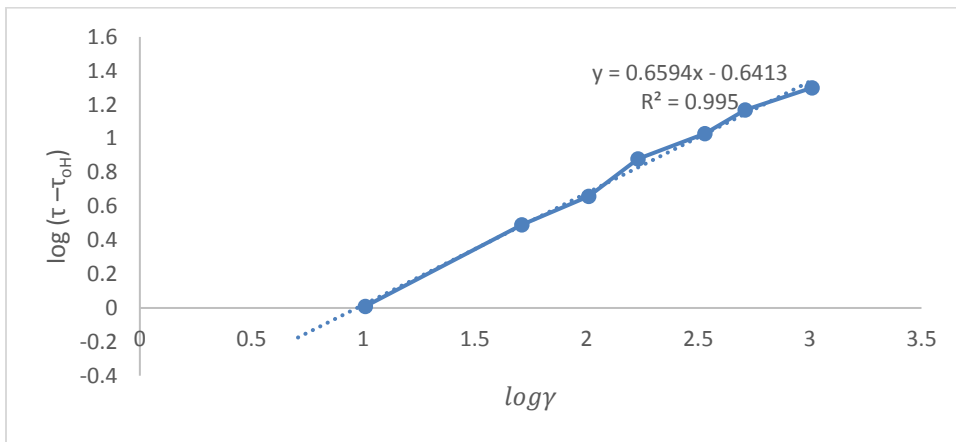


Figure 6: Herschel-Bulkley Rheogram for NC1 + 0.6g PACR

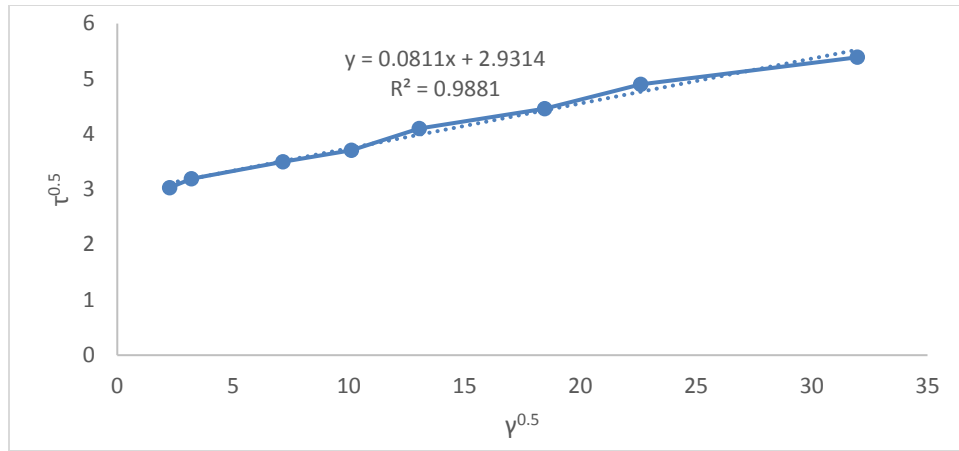


Figure 7: Casson Rheogram for NC1 + 0.6g PACR

Table 4: Stress Values of Different Models for NC1 + 0.6g PACR Mud.

Speed (RPM)	Dial readings (lb/100ft ²)	Shear rate (s ⁻¹)	Measured (Pa)	PLRM (Pa)	BPRM (Pa)	HBRM (Pa)	CRM (Pa)
600	57	1022	29.07	25.93449	24.0822	31.37013	30.57789
300	47	511	23.97	22.36856	21.4761	23.22949	22.74374
200	39	340.60	19.89	20.5136	20.60706	19.93202	19.6417
100	33	170.30	16.83	17.69303	19.73853	15.98755	15.94209
60	27	102.18	13.77	15.86571	19.39112	14.04075	14.09092
30	24	51.09	12.24	13.68421	19.13056	12.25755	12.34299
6	20	10.22	10.2	9.706838	18.92212	10.24502	10.19072
3	18	5.11	9.18	8.372169	18.89606	9.854312	9.71084

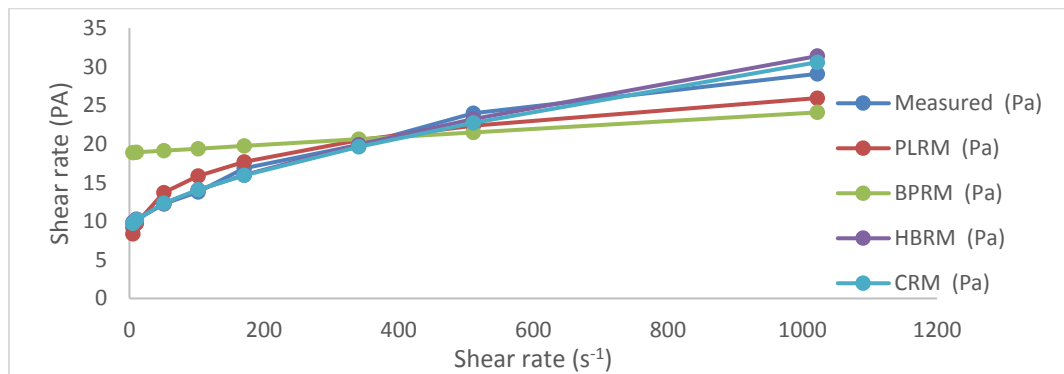


Figure 8: Shear Stress-Shear Rate Graph of Different Models for NC1 + 0.6g PACR

3.3 Analysis of NC2 + 0.6g PACR Mud Sample.

Table 5: Viscometer Readings for NC2 + 0.6g PACR

Speed (RPM)	Dial readings (lb/100ft ²)	Shear stress (τ) (pa)	Shear rate (γ) (s ⁻¹)	logτ	logγ	log (τ - τ _{oH})	τ ^{0.5}	γ ^{0.5}
600	33	16.83	1022	1.23	3.01	1.09	4.10	31.97
300	23	11.73	511	1.07	2.71	0.85	3.42	22.61
200	19	9.69	340.60	0.99	2.53	0.71	3.11	18.46
100	18	9.18	170.30	0.96	2.23	0.66	3.03	13.05
60	15	7.65	102.18	0.88	2.01	0.49	2.77	10.11
30	13	6.63	51.09	0.82	1.71	0.31	2.57	7.15
6	11	5.61	10.22	0.75	1.01	0.01	2.37	3.20
3	9	4.59	5.11	0.66	0.708	-	2.14	2.26

3.3.1 Model Parameters Determination for NC2 + 0.6g PACR

The parameters n and k for the power law rheological model were derived through regression analysis using Equation (8). The resulting plot of log τ versus log γ, as shown in Figure 9, produced a straight line, which is represented by Equation (26):

$$\text{Log}\tau = 0.2176\text{log}\gamma + 0.4871 \tag{26}$$

Therefore, the power law equation for NC2 + 0.6g PACR can be written as:

$$\tau = 3.07\gamma^{0.2176} \tag{27}$$

Equation (27) was then used to calculate the power law stress values presented in Table 6.

The yield stress (τ_o) for the Bingham plastic model was calculated using Equation (7), which yielded a value of 13 lb/100ft². By multiplying this value by 0.51, the result was converted to Pascals. The plastic viscosity was then determined using Equation (6) and found to be 0.0051 mPa-s. Consequently, the Bingham plastic stress equation for NC2 + 0.6g PACR is:

$$\tau = 6.63 + 0.0051\gamma \tag{28}$$

Equation (28) was used to generate the Bingham plastic stresses shown in Table 6.

For the Herschel-Bulkley model, the yield stress τ_{oH} was taken as the Θ₃ yield stress, which is 4.59 Pa. The flow behavior index and consistency index were determined through regression analysis using Equation (10). The resulting plot of log (τ - τ_{oH}) against log γ, as shown in Figure 10, gave the straight line represented by Equation (29):

$$\text{Log} (\tau - \tau_{oH}) = 0.5254\text{log}\gamma - 0.553. \tag{29}$$

Hence the Hershel Bulkley equation for NC + 0.6g PACR is given as

$$\tau = 4.59 + 0.2799 (\gamma^{0.5254}) \tag{30}$$

Eq. (30) was used to generate the Hershel-Buckley stresses shown in table 6.

Lastly, the Casson yield stress (k_{oc}) and the Casson plastic viscosity (k_c) were derived from the plot of $\tau^{0.5}$ versus $\gamma^{0.5}$, as shown in Figure 11. Based on this plot, the Casson equation for NC2 + 0.6g PACR is:

$$\tau^{0.5} = 4.47^{0.5} + 0.00367^{0.5} (\gamma^{0.5}) \tag{31}$$

Equation (31) was used to compute the Casson stresses presented in Table 6.

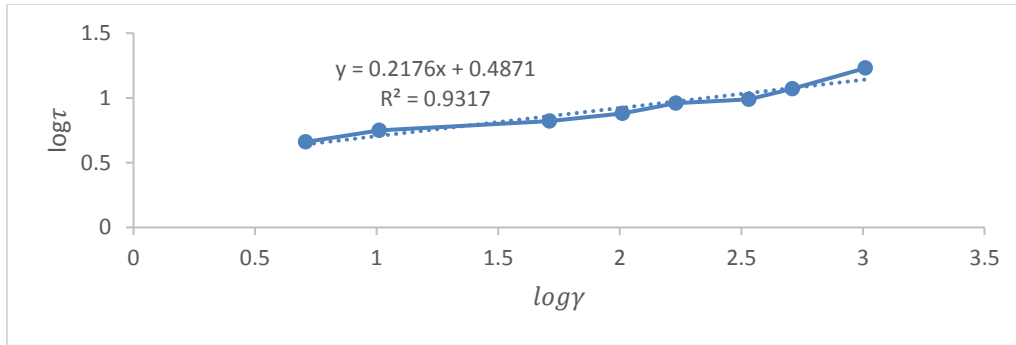


Figure 9: Power law Rheogram for NC2 + 0.6g PACR

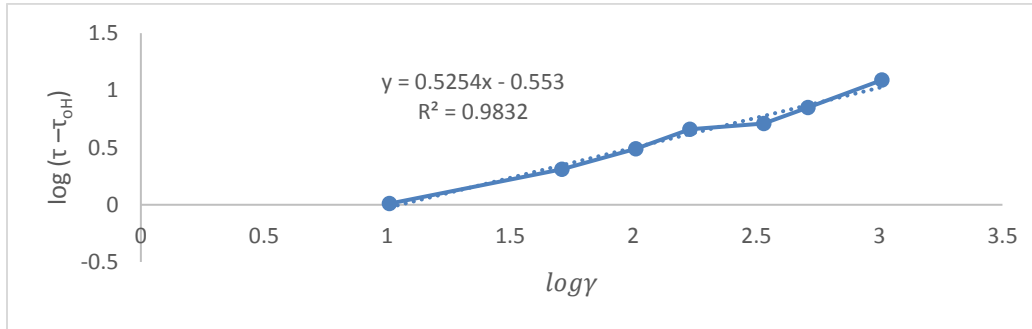


Figure 10: Hershel-Buckley Rheogram for NC2 + 0.6g PACR.

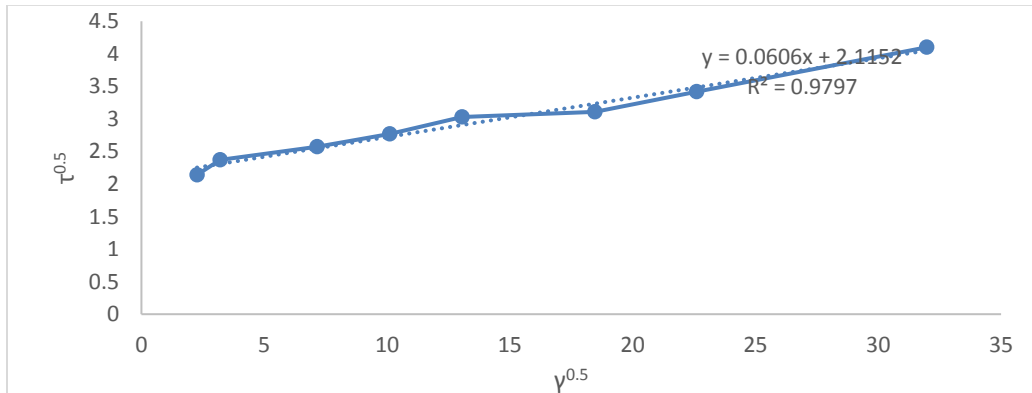


Figure 11: Casson Rheogram for NC2 + 0.6g PACR.

Table 6: Stress Values of Different Models for NC2 + 0.6g PACR Mud.

Speed (RPM)	Dial readings (lb/100ft ²)	Shear rate (s ⁻¹)	Measured (Pa)	PLRM (Pa)	BPRM (Pa)	HBRM (Pa)	CRM (Pa)
600	33	1022	16.83	13.8674	11.8422	15.2601	16.40995
300	23	511	11.73	11.92589	9.2361	12.00323	12.13602
200	19	340.60	9.69	10.91829	8.36706	10.58024	10.44758
100	18	170.30	9.18	9.389678	7.49853	8.751818	8.437907
60	15	102.18	7.65	8.401878	7.151118	7.772173	7.434404
30	13	51.09	6.63	7.225573	6.890559	6.800867	6.488485
6	11	10.22	5.61	5.090904	6.682122	5.539223	5.326429
3	9	5.11	4.59	4.378151	6.656061	5.249489	5.067819

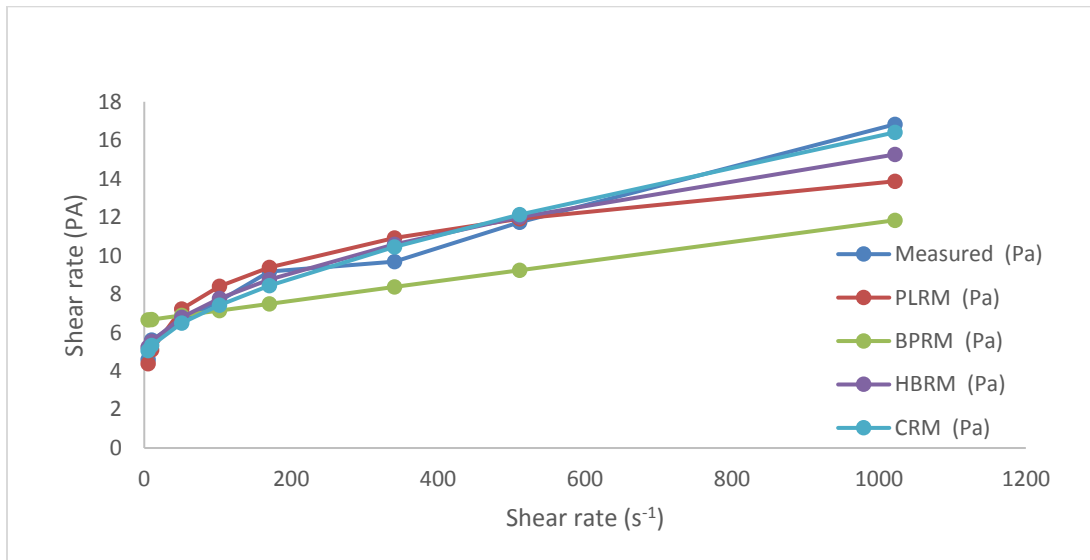


Figure 12: Shear Stress-Shear Rate Graph of Different Models for NC2 + 0.6g PACR

3.4.1 Analysis of NC3 + 0.6g PACR Mud Sample.

Table 7: Viscometer Readings for NC3 + 0.6g PACR.

Speed (RPM)	Dial readings (lb/100ft ²)	Shear stress (τ) (pa)	Shear rate (γ) (s ⁻¹)	$\log \tau$	$\log \gamma$	$\log (\tau - \tau_{oH})$	$\tau^{0.5}$	$\gamma^{0.5}$
600	70	35.7	1022	1.55	3.01	1.36	5.97	31.97

300	60	30.6	511	1.49	2.71	1.25	5.53	22.61
200	52	26.52	340.60	1.42	2.53	1.14	5.15	18.46
100	45	22.95	170.30	1.36	2.23	1.01	4.79	13.05
60	35	17.85	102.18	1.25	2.01	0.71	4.22	10.11
30	30	15.3	51.09	1.18	1.71	0.41	3.91	7.15
6	27	13.77	10.22	1.14	1.01	0.01	3.71	3.20
3	25	12.75	5.11	1.11	0.708	-	3.57	2.26

3.4.1 Model Parameter Determination for NC3 + 0.6g PACR

The parameters n and k for the power law rheological model were derived by plotting $\log \tau$ versus $\log \gamma$, as shown in Figure 13. This produced a straight line, which is represented by the following equation (Equation 32):

$$\text{Log} \tau = 0.1969 \log \gamma + 0.9207 \quad 32$$

Thus, the power law model for NC3 + 0.6g PACR can be written as:

$$\tau = 8.33 \gamma^{0.1969} \quad 33$$

Equation (33) was used to calculate the power law stress values presented in Table 8.

The plastic viscosity was calculated using Equation (6), yielding a value of 0.0051 mPa·s, while the yield stress, obtained from Equation (7), was found to be 25.5 Pa. Therefore, the Bingham Plastic model for NC3 + 0.6g PACR is expressed as:

$$\tau = 25.5 + 0.0051 \gamma \quad 34$$

Equation (34) was applied to generate the Bingham Plastic stresses shown in Table 8.

For the Herschel-Bulkley model, the equation derived from the plot of $\log (\tau - \tau_{oH})$ against $\log \gamma$, as depicted in Figure 14, is:

$$\text{Log} (\tau - \tau_{oH}) = 0.7216 \log \gamma - 0.7265 \quad 35$$

Thus, the Herschel-Bulkley equation for NC3 + 0.6g PACR is:

$$\tau = 12.75 + 0.19 (\gamma^{0.7216}) \quad 36$$

Equation (36) was used to compute the Herschel-Bulkley stresses shown in Table 8.

Lastly, for the Casson model, the equation derived from the plot of $\tau^{0.5}$ versus $\gamma^{0.5}$, as shown in Figure 15, is:

$$\tau^{0.5} = 11.84\gamma^{0.5} + 0.0073\gamma^{0.5}$$

37

Equation (37) was used to calculate the Casson stresses, which are presented in Table 8.

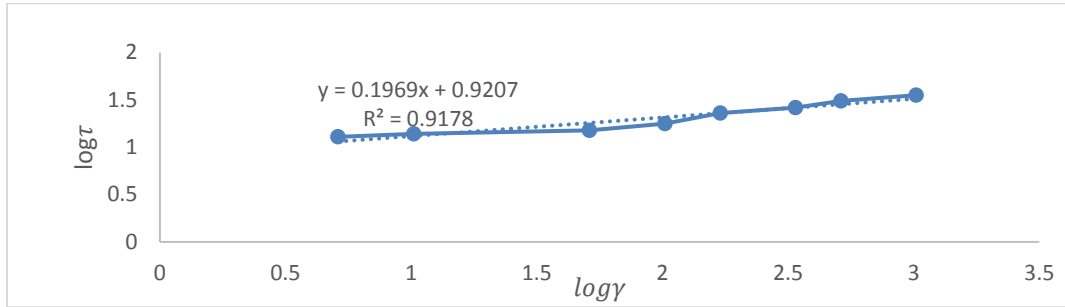


Figure 13: Power law Rheogram for NC3 + 0.6g PACR

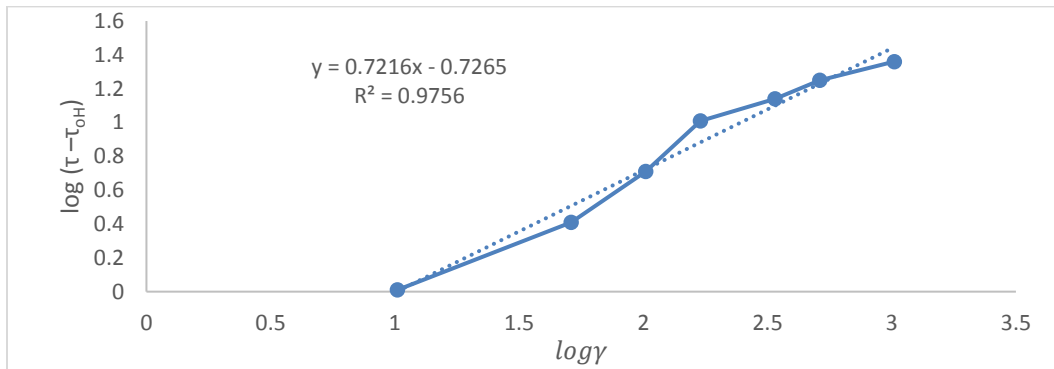


Figure 14: Hershel-Buckley Rheogram for NC2 + 0.6g PACR.

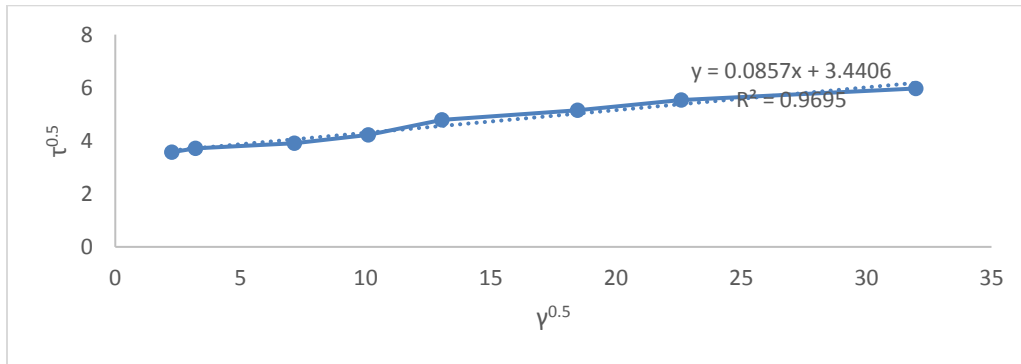


Figure 15: Casson Rheogram for NC3 + 0.6g PACR.

Table 8: Stress Values of Different Models for NC3 + 0.6g PACR Mud.

Speed (RPM)	Dial readings (lb/100ft ²)	Shear rate (s ⁻¹)	Measured (Pa)	PLRM (Pa)	BPRM (Pa)	HBRM (Pa)	CRM (Pa)
600	57	1022	35.7	32.59912	30.7122	40.95807	38.09778

300	47	511	30.6	28.44023	28.1061	29.85607	28.86191
200	39	340.60	26.52	26.25693	27.23706	25.51502	25.17788
100	33	170.30	22.95	22.90716	26.36853	20.49102	20.75636
60	27	102.18	17.85	20.7152	26.02112	18.10442	18.52952
30	24	51.09	15.3	18.07242	25.76056	15.99705	16.41572
6	20	10.22	13.77	13.16455	25.55212	13.76665	13.79432
3	18	5.11	12.75	11.48505	25.52606	13.36652	13.20646

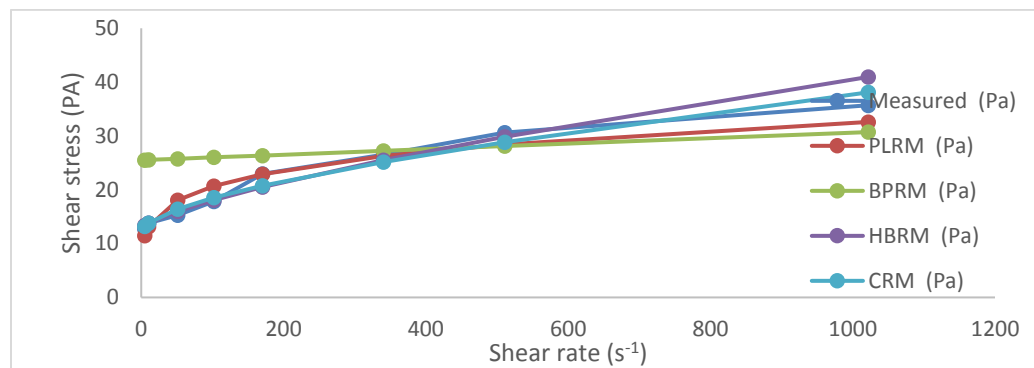


Figure 16: Shear Stress-Shear Rate Graph of Different Models for NC3 + 0.6g PACR

3.5 Result Discussion

Table 2, 4, 6 and 8 presents data for shear rate and corresponding measured shear stresses along with values predicted by four different rheological models: the Power Law Rheological Model (PLRM), Bingham Plastic Rheological Model (BPRM), Herschel-Bulkley Rheological Model (HBRM), and Casson Rheological Model (CRM). These models are widely used in drilling fluid analysis to describe the behavior of non-Newtonian fluids, which are typical in drilling operations. The measured shear stress at different shear rates serves as the benchmark for evaluating the performance of these models. From the table, it can be observed that the shear stress decreases as the shear rate decreases, which is consistent with the behavior of drilling fluids that exhibit shear-thinning characteristics. Based on Figures 4, 8, 12, and 16, which present stress values predicted by various rheological models for NC, NC1, NC2, and NC3, it can be observed that the Bingham Plastic rheological model predicts lower stress values at higher shear rates compared to the measured stress values. However, at lower shear rates, the model predicts higher stress values. This behavior at lower shear rates arises from the inclusion of a yield stress in the Bingham Plastic model.

This yield stress, also known as the Bingham Yield Point (τ_0), represents the minimum stress required for the fluid to begin shearing and this unrealistically high values of computed τ_0 attributed to a major inherent drawback of this model in predicting the shear stress-shear rate behavior of drilling fluids (Adewale et al., 2017). Also, The stress values predicted by the Power Law rheological model are lower than the measured values at both high and low shear rate conditions and this is also in agreement with Adewale et al., (2017) in their research article titled “Selecting the Most Appropriate Model for Rheological Characterization of Synthetic Based Drilling Mud” and this can be attributed by the partial reconstruction of the fluid’s microstructure, which had been disrupted by prior shear (Wei et al., 2022). Hence, the results of the Power law rheological model agrees, with Ba et al., (2018), This is due to its inability to accurately capture the behavior of the drilling fluid at extremely low shear rates in the annulus or

extremely high shear rates at the bit. From Figures 4, 8, 12, and 16, it is clear that the stress values predicted by the HBRM align well with the measured stress values.

Hemphil et al. (1993) and Adewale et al. (2017) highlighted that the Yield Power Law Model (HBRM) offers several advantages over the Bingham Plastic Rheological Model (BPRM) and the Power Law Rheological Model (PLRM), particularly due to its higher accuracy in describing mud behavior across a wide range of shear rates. The improved precision of the HBRM can also be attributed to its ability to account for both the yield point (Bingham Plastic) and the non-linear relationship between shear stress and shear rate, as noted by Adewale et al. (2017). For the Casson Rheological Model (CRM), the overall trend indicates that it is the most reliable model across all stress ranges, as it consistently aligns well with the measured values, showing no significant over- or under-predictions, as illustrated in Figures 4, 8, 12, and 16 for all four mud samples. The graphs demonstrate that this model provides the most accurate data at both high and low shear rate conditions. This accuracy is attributed to the correction factor applied to the yield stress and plastic viscosity, as noted by Adewale et al. (2017). In all, the consistent underestimation at high shear rates and over estimation at low shear rates by BPRM indicates that it might not capture the non-linear fluid behavior effectively, particularly at higher shear rates where deviations are more pronounced. HBRM, on the other hand, tends to overestimate shear stress, especially at high shear rates, which could lead to an over prediction of the fluid's viscosity. PLRM provides reasonable approximations across the shear rate range, but its slight deviations at higher rates show limitations in capturing the full stress behavior. CRM stands out as the most accurate model overall, closely matching the measured shear stress values across the entire range.

In the context of drilling fluids, accurate shear stress predictions are essential to ensure effective fluid flow, lubrication, and cuttings transport during drilling operations. Models that under predict stress, like BPRM, may result in incorrect viscosity estimations, leading to operational inefficiencies. Conversely, overestimations, as seen with HBRM, could lead to excessive pressure losses and increased energy requirements. CRM's consistent performance suggests it is the most suitable model for predicting shear stress under varying shear rates, making it a reliable tool for optimizing drilling fluid performance and this report and findings was in agreement with Adewale et al. (2017).

Table 9 Absolute Average Percentage Error (ϵ_{AAP}) of the Rheological Models

Mud Samples	PRLM	PBRM	HBRM	CRM
NC	8.41786	43.20561	6.369951	5.540541
NC1	8.297946	42.11455	3.26438	3.234073
NC2	8.364122	19.68012	5.664074	5.28458
NC3	8.176579	42.4544	5.31308	5.233931

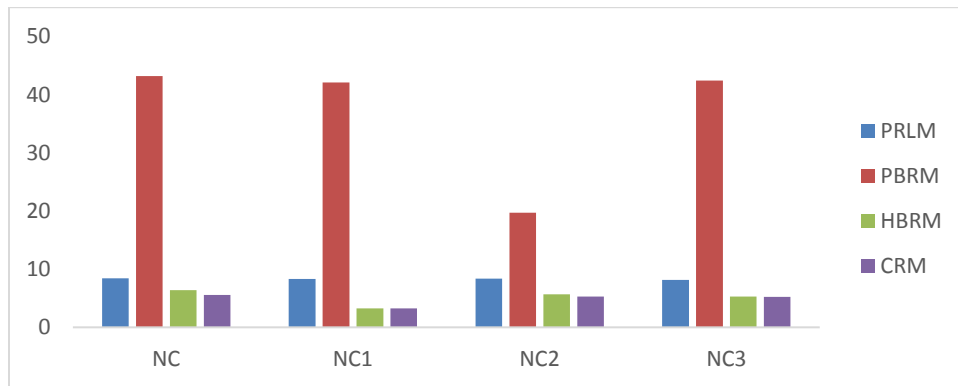


Figure 17: Absolute Average Percentage Error in Rheological Models

3.5.1 Error Analysis

Table 9 and figure 17 shows the evaluation of the Absolute Average Percentage Error (AAPE) of various rheological models (PRLM, PBRM, HBRM, CRM) for different mud samples, where lower AAPE values indicate higher accuracy and better model performance. PRLM consistently shows relatively high AAPE values across the samples, such as 8.41786 for NC and 8.297946 for NC1, indicating less accuracy in predicting the rheological behavior compared to HBRM and CRM models. PBRM performs the poorest, exhibiting the highest AAPE values, such as 43.20561 for NC and 42.11455 for NC1, suggesting its unreliability in modeling the rheological properties. HBRM, on the other hand, shows significantly lower AAPE values, such as 6.369951 for NC and 3.26438 for NC1, indicating improved accuracy over PRLM and PBRM. CRM demonstrates the lowest AAPE values across most samples, for example, 5.540541 for NC and 3.234073 for NC1, making it the most accurate and reliable model among those compared. Overall, the comparison highlights that CRM outperforms the other models with the least deviation, followed closely by HBRM, while PRLM and particularly PBRM exhibit larger errors, making them less suitable for predicting the rheological behavior of these mud samples and this results of error analysis was in agreement with the findings of Adewale et al., (2017), in their research article titled “Selecting the most appropriate model for rheological characterization of synthetic based drilling mud”

Table 10 Standard Deviation of the Average Percentage Error for Rheological Models.

Mud Samples	PRLM	PBRM	HBRM	CRM
NC	7.233173	39.32119	4.191358	3.853428
NC1	4.104296	37.55928	3.163145	2.341603
NC2	5.386464	13.10984	4.768432	3.109538
NC3	6.493866	38.17961	4.961843	2.821159

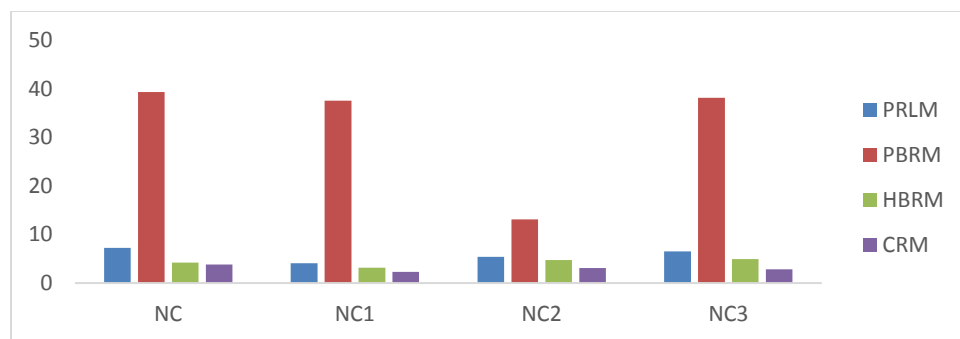


Figure 18: Standard Deviation of Average Percentage Error for Rheological Models.

Table 10 and figure 18 presents the standard deviation of the absolute average percentage error for various rheological models, including PRLM, PBRM, HBRM, and CRM, across different mud samples. Each model exhibits varying degrees of accuracy depending on the mud sample tested. For instance, in sample NC, the PBRM model demonstrates the largest error with a value of 39.32, followed by PRLM with a value of 7.23. HBRM with a value of 4.19 on the other hand, shows significantly lower value of SD_{AAPE} while CRM achieves the lowest error at 3.85, indicating CRM's superior predictive performance for this case.

A similar trend can be observed for NC1, where PBRM again shows a significantly higher error at 37.56 compared to CRM, which achieves the lowest error of 2.34 closely followed by HBRM with a value of 3.16 and PRLM with a value of 4.10. In NC2, the deviation for PBRM drops to 13.11, but it remains higher than CRM's 3.10. Meanwhile, HBRM records values consistently lower than PRLM and PBRM, with errors ranging between 3.16 and 4.96 across samples. Finally, for NC3, the PBRM model records another high error value of 38.18, while CRM achieves a relatively low value of 2.82. Overall, the CRM model demonstrates the most consistent and lowest standard deviation of errors among the tested rheological models, reflecting its robust performance. Conversely, PBRM consistently shows the highest errors, indicating a lack of accuracy in predicting the rheological behavior of the mud samples. The PRLM model, while better than PBRM, still exhibits higher errors compared to HBRM and CRM. These findings suggest that CRM is the most reliable model for predicting the rheological properties of these mud

samples, while PBRM requires further improvement to minimize its error margin and enhance prediction accuracy. This comparison highlights the varying reliability of the models and underscores the importance of selecting the appropriate model based on the specific conditions and error tolerance of the application. This results of error analysis was in agreement with the findings of Adewale et al., (2017), in their research article titled “Selecting the Most Appropriate Model for Rheological Characterization of Synthetic Based Drilling Mud

4.0. Conclusion

This paper outlines the rheological behavior of water-based drilling mud using four rheological models: Power Law Model, Bingham Plastic Model, Herschel-Bulkley Model, and Casson Model. Among these, CRM exhibited the minimum AAPE and standard deviation for all the samples: NC, NC1, NC2, and NC3. HBRM also showed a good approximation since the calculated points were reasonably close to the measured ones. On the other hand, a moderately good approximation was given by PLRM, and the poorest performance was given by BPRM, especially for low and high values of shear rate. Hence, it is the least reliable. The strength of this paper is that CRM accounted very well for the rheological characteristics of water-based drilling mud. Thus, it can be taken as a model for optimization studies aimed at enhancing the performance of drilling fluids. Results obtained give some important hints when developing rheological models with the aim of improving operational efficiency in drilling.

5.0 Funding

The research work was supported by the tertiary Education Trust Fund, Nigeria through the Institution Based Research grant (IBR): TETFUND Research Projects (RP) Intervention Funds, DATED; 11TH JUNE, 2024. Ref: NAU/TETFC/IBR/2024/VOL.V/16

Competing interests

Authors have declared that no competing of interest exist.

References

- Adewale, F. J., Lucky, A. P., Oluwabunmi, A. P., & Boluwaji, E. F. 2017. Selecting the most appropriate model for rheological characterization of synthetic based drilling mud. *Int. J. Appl. Eng. Res*, 12(18), 7614-7629.
- Aftab, A. A. R. I., Ismail, A. R., Ibupoto, Z. H., Akeiber, H., & Malghani, M. G. K. 2017. Nanoparticles based drilling muds a solution to drill elevated temperature wells: A review. *Renewable and Sustainable Energy Reviews*, 76, 1301-1313.
- Fakhari, N. 2022. *A mud design to improve water-based drilling in clay rich formation* (Doctoral dissertation, Curtin University).
- Anawe, P. A. L., & Folayan, J. A. 2018. Data analyses on temperature-dependent behaviour of water based drilling fluid rheological models. *Data in brief*, 21, 289-298.
- Ba, Y., Wang, N., Liu, H., Li, Q., & He, G. 2018. Regularized lattice Boltzmann model for immiscible two-phase flows with power-law rheology. *Physical Review E*, 97(3), 033307.
- Chen, H. 2022. Optimization of Drilling Fluid Rheological Properties for Improved Cuttings Transport and Dynamic Filtration Loss Control Performance: A Comparative Study of the Fluid Viscoelasticity versus the Shear Viscosity Effects.
- Chu, Q., & Lin, L. 2019. Effect of molecular flexibility on the rheological and filtration properties of synthetic polymers used as fluid loss additives in water-based drilling fluid. *RSC advances*, 9(15), 8608-8619.
- Chukwuemeka, A. O., Amede, G., & Alfazazi, U. 2017. A Review Of Wellbore Instability During Well Construction: Types, Causes, Prevention And Control. *Petroleum & Coal*, 59(5).

- Deng, S., Kang, C., Bayat, A., Kuru, E., Osbak, M., Barr, K., & Trovato, C. 2020. Rheological properties of clay-based drilling fluids and evaluation of their hole-cleaning performances in horizontal directional drilling. *Journal of Pipeline Systems Engineering and Practice*, 11(3), 04020031.
- Hemphill, T., Campos, W., & Pilehvari, A. 1993. Yield-power law model more accurately predicts mud rheology. *Oil and Gas Journal (United States)*, 91(34).
- Irgens, F. 2014. *Rheology and non-newtonian fluids* (Vol. 1). New York: Springer International Publishing.
- James O. O., Adediran, M.M., Adekola, F.A., Adebunmi, E.O. and Adekeye, J.I.D., 2008. Beneficiation and characterization of a bentonite from north-eastern Nigeria. *Journal of the North Carolina Academy of Science*, 124(4), 154–158
- Klungtvedt, K. R. 2023. Drilling fluid additives for wellbore strengthening and reservoir protection.
- Krishna, K. V., Swathi, K., Hemalatha, M., & Mohan, S. V. 2019. Bioelectrocatalyst in Microbial Electrochemical Systems and Extracellular Electron Transport. In *Microbial Electrochemical Technology* (pp. 117-141). Elsevier.
- Mitsoulis, E., & Tsamopoulos, J. 2017. Numerical simulations of complex yield-stress fluid flows. *Rheologica Acta*, 56, 231-258.
- Nollet, L. M., & Toldrá, F. Nollet 2015-Handbook of Food Analysis. pdf
- Pedrosa, C., Saasen, A., & Ytrehus, J. D. 2021. Fundamentals and physical principles for drilled cuttings transport—Cuttings bed sedimentation and erosion. *Energies*, 14(3), 545.
- Picchi, D., Poesio, P., Ullmann, A., & Brauner, N. 2017. Characteristics of stratified flows of Newtonian/non-Newtonian shear-thinning fluids. *International Journal of Multiphase Flow*, 97, 109-133.
- Rostami, A. 2017. Prediction and evaluation of annular pressure in horizontal directional drilling.
- Sarsenbaevna, B. U., & Ospanovich, K. M. 2024. The Process Of Drilling Oil And Gas Wells. *The American Journal of Applied sciences*, 6(06), 49-52.
- Sharma, P., & Kudapa, V. K. 2021. Rheological study of fluid flow model through computational flow dynamics analysis and its implications in mud hydraulics. *Materials Today: Proceedings*, 47, 5326-5333.
- Wei, Y., Li, R., & Zhang, H. 2022. Measures of the yield stress fluids oriented for dysphagia management using steady-state shear, transient shear, and large-amplitude oscillatory shear (LAOS). *Physics of Fluids*, 34(12).